

Article

Surface Scattering Expansion of the Casimir–Polder Interaction for Magneto-Dielectric Bodies: Convergence Properties for Insulators, Conductors, and Semiconductors

Giuseppe Bimonte ^{1,*} and Thorsten Emig ²

¹ Dipartimento di Fisica E. Pancini, Università di Napoli Federico II, Complesso Universitario di Monte S. Angelo, Via Cintia, I-80126 Napoli, Italy

² Laboratoire de Physique Théorique et Modèles Statistiques, CNRS UMR 8626, Université Paris-Saclay, CEDEX, 91405 Orsay, France; thorsten.emig@cnrs.fr

* Correspondence: giuseppe.bimonte@na.infn.it

† INFN Sezione di Napoli, I-80126 Napoli, Italy.

Abstract: Fluctuation-induced forces are a hallmark of the interplay between fluctuations and geometry. We recently proved the existence of a multi-parametric family of exact representations of Casimir and Casimir–Polder interactions between bodies of arbitrary shape and material composition, admitting a multiple scattering expansion (MSE) as a sequence of inter-body and intra-body multiple wave scatterings. The approach requires no knowledge of the scattering amplitude (T-matrix) of the bodies. In this paper, we investigate the convergence properties of the MSE for the Casimir–Polder interaction of a polarizable particle with a macroscopic body. We consider representative materials from different classes, such as insulators, conductors, and semiconductors. Using a sphere and a cylinder as benchmarks, we demonstrate that the MSE can be used to efficiently and accurately compute the Casimir–Polder interaction for bodies with smooth surfaces.

Keywords: Casimir–Polder force; scattering expansion; surface integral equation; silicon; gold; polystyrene



Citation: Bimonte, G.; Emig, T. Surface Scattering Expansion of the Casimir–Polder Interaction for Magneto-Dielectric Bodies: Convergence Properties for Insulators, Conductors, and Semiconductors. *Physics* **2024**, *6*, 194–205. <https://doi.org/10.3390/physics6010014>

Received: 6 December 2023

Revised: 2 January 2024

Accepted: 9 January 2024

Published: 9 February 2024



Copyright: © 2024 by the authors. Licensee MDPI, Basel, Switzerland. This article is an open access article distributed under the terms and conditions of the Creative Commons Attribution (CC BY) license (<https://creativecommons.org/licenses/by/4.0/>).

1. Introduction

Following the seminal paper of Hendrick Casimir, who discovered that two discharged perfectly conducting parallel plates at zero temperature attract each other with a force originating from quantum fluctuations of the electromagnetic (EM) field [1], Evgeny Lifshitz successfully used the then-new field of fluctuational electrodynamics to compute the Casimir force between two parallel, infinite surfaces of dispersive and dissipative dielectric bodies at finite temperature [2]. By taking the dilute limit for one of the two bodies, Lifshitz could also compute the Casimir–Polder (CP) force between a small polarizable particle and a planar surface. Lifshitz’s results remained unsurpassed for a long time, because it was not understandable how to extend his computation beyond planar surfaces. Computing the Casimir and CP interactions in non-planar geometries is actually a notoriously complicated problem, due to the collective and non-additive character of dispersion forces. For many years, the only method to estimate dispersion forces in non-planar setups was the Derjaguin additive approximation [3], the so-called Proximity Force Approximation (PFA), which expresses the Casimir force between two non-planar surfaces as the sum of the forces between pairs of small opposing planar portions of the surfaces. Because of its simplicity, the PFA is still often used to interpret modern experiments with curved bodies; for reviews, see [4–9].

A significant step forward in the study of curved surfaces was made in the 1970s by Dieter Langbein, who used scattering methods to study the Casimir interaction between spheres and cylinders [10]. The remarkable study of Langbein went quite unnoticed, and it was quickly forgotten. A new wave of strong interest in the problem arose at the beginning

of this century, spurred by modern precision experiments on the Casimir effect [11–18]. The intense theoretical efforts that were put forward culminated in the discovery of the scattering Formula [19–21]. According to this formula, which was initially devised for non-planar mirrors [22,23], the interaction between dielectric bodies is expressed in terms of their scattering amplitude, known as T-operator. While this formalism has been the basis of the theoretical advancements made in recent years, its practical use is limited by the feature that the T-operator is known only for highly symmetric bodies, such as spheres and cylinders, or for a few perfectly conducting shapes [24]. Remarkably enough, it has been found that the scattering formula can be computed exactly for the sphere–plate and sphere–sphere systems for Drude conductors in the high temperature limit [25,26]. By improved numerical methods, the scattering formula for a dielectric sphere and a plate at finite temperature can be computed with high precision also for experimentally relevant small separations [27]. To note, however, is that the precision of current experiments using a simple enough sphere–plate geometry has not yet reached the point where deviations from the PFA to be observed.

As mentioned above, the practical use of the scattering approach is limited to the few simple shapes for which the scattering amplitude is known. A more fundamental limitation of the scattering approach is that interlocked geometries evade this method due to lack of convergence of the mode expansion [28]. The necessity of theoretical formulations for a precise force computation in complex geometries has become urgent lately, because recent experiments using micro-fabricated surfaces [28–30] have indeed shown large deviations from the PFA. Theoretical progress has been made for the special case of dielectric rectangular gratings by using a generalization of the Rayleigh expansion in Refs. [31–33]. On a different route, a general approach has been devised for gently curved surfaces, for which a gradient expansion can be used to obtain first order curvature corrections to the proximity force approximation for the Casimir force [34–37]. In this approach, the Casimir energy is expanded in powers of derivatives of the height functions of the surfaces, whose coefficients can be computed analytically by matching the gradient expansion with the perturbative expansion of the energy in the common domain of validity of both expansions.

A breakthrough occurred in 2013 [38] when it was shown that surface integral-equations methods [39,40], which have been used for a long time in computational electromagnetism, can also be used to compute, at least in general, Casimir interactions for arbitrary arrangements of any number of (homogeneous) magneto-dielectric bodies of any shape. The formulation in [38] expresses Casimir forces and energies as traces of certain expressions involving a surface operator, evaluated along the imaginary frequency axis. The surface operator consists of linear combinations with constant coefficients of free Green tensors of the EM field of $N + 1$ *homogeneous* infinite media, having the permittivities of the N bodies, and of the medium surrounding them. A potential problem with the approach of Ref. [38] is that the expression for the Casimir interaction contains the inverse of the surface operator, which has to be computed numerically by replacing the continuous surfaces with a suitable discrete mesh. This operation replaces the surface operator by a large matrix whose elements involve double surface integrals of the free Green tensors over all pairs of small surface elements composing the mesh. The generation of the matrix is time consuming because of the strong inverse-distance cubed singularity of the surface operator in the coincidence limit. In addition, the size of the non-sparse matrix for sufficiently fine meshes can quickly exceed the memory-usage limit, preventing the matrix numerical inversion.

Inspired by earlier papers of Roger Balian and Bertrand Duplantier on the Casimir effect for perfect conductors [41,42], we have recently derived a multiple scattering expansion (MSE) of Casimir and CP interactions for magneto-dielectric bodies of arbitrary shape [43,44]. Similar to Ref. [38], in the MSE approach the interactions have the form of traces of expressions involving the inverse of a surface operator, $\mathbb{M}(i\zeta)$, evaluated along the imaginary frequency axis. A crucial difference with respect to Ref. [38] is that the MSE kernel \mathbb{M} has the form of a Fredholm surface integral operator of the second kind,

$$\mathbb{M} = \mathbb{I} - \mathbb{K} . \quad (1)$$

Here, \mathbb{I} and \mathbb{K} represent the identity and the surface scattering operator (SSO), respectively.

The Fredholm form implies that the inverse \mathbb{M} can be computed as a power (Neumann) series,

$$\mathbb{M}^{-1} = \mathbb{I} + \mathbb{K} + \mathbb{K}^2 + \dots, \quad (2)$$

which converges, provided that the spectral radius of \mathbb{K} is less than one. Hence, one obtains an expansion of Casimir and CP interaction in the powers of \mathbb{K} , which can be interpreted as an expansion in the number of scatterings off the surfaces of the bodies. Specifically, the MSE has the form of an iterated series of surface integrals of elementary functions, running over the surfaces of the bodies. Let us note that a particular choice of the free coefficients in the kernel \mathbb{K} exists, such that the kernel has a weak $1/|\mathbf{u} - \mathbf{u}'|$ singularity, where \mathbf{u} and \mathbf{u}' are the points on the surface. The weak singularity feature should simplify and expedite numerical evaluations on a mesh. An additional advantage implied by the MSE, if implemented on a mesh, is that one does not need to store the matrix for \mathbb{K} in memory, since its elements can be computed at the moment of performing the matrix multiplication.

Considering specifically the CP interaction of a polarizable particle with a dielectric body, let us note that the problem has been studied by many authors in the past, using a variety of methods. A distinction can be made between approaches devised for bodies of special shapes, as opposed to formulations that can handle bodies of arbitrary shapes. The first group includes spheres and cylinders, for which the scattering formula leads to a simple exact expression for the CP energy in terms of the exactly known T-operator [45–48]. This group also includes the computation of the exact CP interaction between an atom and a rectangular dielectric grating [32,49], based on the Rayleigh expansion. Regarding the second group of approaches, it has been shown [50,51] that the gradient expansion [34–37] can be used to compute the leading and the next-to-leading curvature corrections beyond the PFA for the CP energy of an atom in front of a gently curved surface of any shape. A numerical time-domain approach to compute the CP interaction of an atom with an arbitrary micro-structured body has been recently discussed [52]. Let us stress that this elegant approach offers the possibility of dealing with a broad range of dielectric materials, including inhomogeneous and possibly non-local materials.

In this paper, we investigate the power of the MSE in the computation of CP interactions. In its present formulation, the MSE allows one to deal with homogeneous and local magneto-dielectric bodies of any shapes, which is the situation of interest in experiments carried out so far. In [43], we showed that only a few terms of the MSE are sufficient to obtain a fairly accurate estimate of the Casimir energy between a Si wedge and a Au plate. The purpose of the present study is to investigate the convergence properties of the MSE for the CP interaction between a polarizable isotropic particle and a dielectric body. We use as benchmarks two shapes that can be solved exactly by using the scattering approach, namely a sphere or a cylinder. We consider different types of materials for the sphere and the cylinder in order to see how the material properties of the bodies affect the rate of convergence of the MSE. We demonstrate that, in all the cases considered, the MSE converges quite fast and uniformly with respect to the particle-surface separation. Since there is no reason to expect that the convergence properties of the MSE bring whatever difference for bodies that are smooth deformations of a sphere or a cylinder, we argue that the findings of the current study imply that the MSE can be used to efficiently compute the CP interactions for compact and non-compact dielectric bodies with smooth surfaces of an arbitrary shape.

2. Casimir–Polder Energy of a Polarizable Particle and a Magneto-Dielectric Body

We study the CP interaction between a small polarizable particle and a magneto-dielectric body (see Figure 1). The optical response of the particle is described by its (complex) electric, $\alpha(\omega)$, and magnetic, $\beta(\omega)$, polarizability tensors, where ω is the fre-

quency. It is known [6,44] that the CP energy can be expressed in terms of the scattering Green tensor $\Gamma(\mathbf{r}, \mathbf{r}')$ evaluated at the particle's position \mathbf{r}_0 , as

$$E_{CP} = -4\pi k_B T \sum_{n=0}^{\infty} \kappa_n \sum_{i,j=1}^3 \left[\alpha_{ij}(i \zeta_n) \Gamma_{ij}^{(EE)}(\mathbf{r}_0, \mathbf{r}_0; \kappa_n) + \beta_{ij}(i \zeta_n) \Gamma_{ij}^{(HH)}(\mathbf{r}_0, \mathbf{r}_0; \kappa_n) \right], \quad (3)$$

where k_B is Boltzmann constant, T is the temperature, $\zeta_n = 2\pi n k_B T / \hbar$, with \hbar the reduced Planck's constant and $n = 0, 1, 2 \dots$, are the Matsubara frequencies, $\kappa_n = \zeta_n / c$ with c the speed of light, the prime in the sum indicates that the $n = 0$ terms has to be taken with a weight of 1/2. The superscripts 'EE' and 'HH' denote the electric and the magnetic fields, respectively. Here, only one scattering at the particle is considered, which is completely justified for particles that are much smaller than the distance from the surface, d . However, multiple scatterings at the body need to be considered. Using the surface integral-equation formulation of EM scattering by a dielectric body [44], one can show that $\Gamma(\mathbf{r}, \mathbf{r}')$ can be expressed as a surface integral extending over the surface, S , of the body,

$$\Gamma(\mathbf{r}, \mathbf{r}') = \int_S ds_{\mathbf{u}} \int_S ds_{\mathbf{u}'} \mathbb{G}_0(\mathbf{r}, \mathbf{u})(\mathbb{I} - \mathbb{K})^{-1}(\mathbf{u}, \mathbf{u}') \mathbb{M}(\mathbf{u}', \mathbf{r}'), \quad (4)$$

where $\mathbb{K}(\mathbf{u}, \mathbf{u}')$ denotes the following SSO,

$$\mathbb{K}(\mathbf{u}, \mathbf{u}') = 2\mathbb{P}(\mathbb{C}^i + \mathbb{C}^e)^{-1} \mathbf{n}(\mathbf{u}) \times \left[\mathbb{C}^i \mathbb{G}_1(\mathbf{u}, \mathbf{u}') - \mathbb{C}^e \mathbb{G}_0(\mathbf{u}, \mathbf{u}') \right], \quad \mathbb{P} = \begin{pmatrix} 0 & -1 \\ 1 & 0 \end{pmatrix}, \quad (5)$$

$\mathbb{M}(\mathbf{u}, \mathbf{u}')$ is the surface operator,

$$\mathbb{M}(\mathbf{u}, \mathbf{r}) = -2\mathbb{P}(\mathbb{C}^i + \mathbb{C}^e)^{-1} \mathbb{C}^e \mathbf{n}(\mathbf{u}) \times \mathbb{G}_0(\mathbf{u}, \mathbf{r}), \quad (6)$$

In Equations (4)–(6), \mathbb{G}_0 and \mathbb{G}_1 are the empty-space Green tensors for the homogenous media with the permittivities ϵ_0 and ϵ_1 and the permeabilities μ_0 and μ_1 , respectively (see Appendix E of Ref. [44] for the definition of \mathbb{G}_0 and \mathbb{G}_1), while $\mathbf{n}(\mathbf{u})$ is the outward unit normal vector to the surface S at point \mathbf{u} . The action $\mathbf{n}(\mathbf{u}) \times$ on the 3×3 matrices $\mathbb{G}_1^{(pq)}$ and $\mathbb{G}_0^{(pq)}$ ($p, q \in \{E, H\}$) is respectively defined by $(\mathbf{n}(\mathbf{u}) \times \mathbb{G}_1^{(pq)})\mathbf{v} \equiv \mathbf{n}(\mathbf{u}) \times (\mathbb{G}_1^{(pq)}\mathbf{v})$ and $(\mathbf{n}(\mathbf{u}) \times \mathbb{G}_0^{(pq)})\mathbf{v} \equiv \mathbf{n}_\sigma(\mathbf{u}) \times (\mathbb{G}_0^{(pq)}\mathbf{v})$, for any vector \mathbf{v} . To note is that \mathbb{K} and \mathbb{M} depend on four arbitrary coefficients, which must form two invertible diagonal 2×2 matrices, \mathbb{C}^i and \mathbb{C}^e .

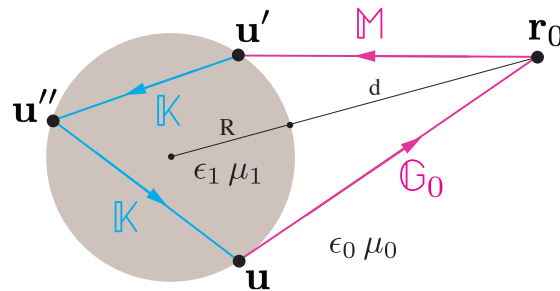


Figure 1. Configuration of a dielectric body (sphere, cylinder) of radius R with the permittivity ϵ_1 and permeability μ_1 interacting with a polarizable particle at position \mathbf{r}_0 outside the object at a distance d from the surface. ϵ_0 and μ_0 denote, respectively, the permittivity and permeability of the surrounding medium. \mathbb{M} , \mathbb{G}_0 and \mathbb{K} are the operators of the multiple scattering expansion. \mathbf{u} , \mathbf{u}' and \mathbf{u}'' mark some positions on the surface of the dielectric body. The arrows denote ordering of the operators. See text for more details.

The existence of an MSE follows from the Fredholm type of the operator $(\mathbb{I} - \mathbb{K})^{-1}$ in Equation (4), which permits an expansion of $\Gamma(\mathbf{r}, \mathbf{r}')$ in powers of \mathbb{K} . This in turn leads to an MSE expansion of the CP energy in Equation (3) in terms of the number of scatterings at

the surface of the body. It is useful to show the first terms of the MSE of the CP energy for the simple case of a particle having an isotropic electric polarizability, $\alpha_{ij} = \alpha \delta_{ij}$ with δ_{ij} the Kronecker delta, and a negligible magnetic polarizability, β ,

$$E_{CP} = -4\pi k_B T \sum_{n=0}^{\infty} \kappa_n \alpha(i \xi_n) \left\{ \sum_{p=E,H} \int_S ds_{\mathbf{u}} \text{tr} \left[\mathbb{G}_0^{(Ep)}(\mathbf{r}_0, \mathbf{u}; \kappa_n) \mathbb{M}^{(pE)}(\mathbf{u}, \mathbf{r}_0; \kappa_n) \right] + \sum_{p,q=E,H} \int_S ds_{\mathbf{u}} \int_S ds_{\mathbf{u}'} \text{tr} \left[\mathbb{G}_0^{(Ep)}(\mathbf{r}_0, \mathbf{u}; \kappa_n) \mathbb{K}^{(pq)}(\mathbf{u}, \mathbf{u}'; \kappa_n) \mathbb{M}^{(qE)}(\mathbf{u}', \mathbf{r}_0; \kappa_n) \right] \right\} + \dots, \quad (7)$$

where the symbol 'tr' denotes a trace over the tensor spatial indices. Since the kernels \mathbb{K} and \mathbb{M} are combinations of free-space Green tensors \mathbb{G}_0 and \mathbb{G}_1 , which are elementary functions of the coordinates, it is understandable that the CP energy involves an iterated series of integrals of elementary functions running over the surface, S , of the body. Since the Green tensors decay exponentially with distance for imaginary frequencies, one immediately sees from Equation (7) that the CP interaction is dominated by the region of the surface that is most closer to the particle. However, one notes that, for the classical term $n = 0$, the Matsubara frequency vanishes and the operators decay only according to a power law.

3. Equivalent Expressions of the SSO

It has to be noticed that different choices of the matrices for the interior, \mathbb{C}^i , and the exterior, \mathbb{C}^e , coefficients lead to *equivalent* SSO, in the sense that the right-hand side of Equation (4) provides different representations of the same scattering tensor for all coefficients [44], given that neither the interior nor the exterior matrices vanish, and that the sum $\mathbb{C}^i + \mathbb{C}^e$ is invertible. This in turn also implies that the CP energy is independent of the values of these coefficients. However, at any *finite* order of the MSE, the CP energy does depend on the chosen coefficients, which implies that the *rate of convergence* of the MSE depends in general on this choice. This important property gives one the possibilities of optimizing convergence of the MSE by suitably choosing the coefficients, dependent on the optical properties of the surfaces. Among the infinite number of the choices for the coefficients, there are two cases which we consider of most importance and describe in detail here.

C1. When the two surface positions, \mathbf{u} and \mathbf{u}' , are close one to another, the SSO has, in general, a $1/|\mathbf{u} - \mathbf{u}'|^3$ singularity. However, a unique choice of the coefficients exists [53], for which the singularity is reduced to a weaker $1/|\mathbf{u} - \mathbf{u}'|$ divergence. The coefficient matrices ensuring this remarkable property are

$$\mathbb{C}^i = \text{diag}(\epsilon_1, \mu_1), \quad \mathbb{C}^e = \text{diag}(\epsilon_0, \mu_0). \quad (8)$$

The corresponding surface operator \mathbb{K} has unique mathematical properties (see Section 6 of Ref. [44]).

C2. A fully asymmetric, material independent choice of coefficient matrices is

$$\mathbb{C}^i = \text{diag}(1, 0), \quad \mathbb{C}^e = \text{diag}(0, 1). \quad (9)$$

For good conductors, one observes relatively fast convergence of the MSE with this choice what is consistent with the observation made in Ref. [42].

4. Results and Discussion

The MSE of the CP energy (7) converges if all eigenvalues of the SSO \mathbb{K} are less than 1 in modulus which to be called here the boundedness property. No a general bound on the eigenvalues of \mathbb{K} was possible to be derived. However, we can prove [44] the boundedness property for the choice case C1 of the coefficients (see Equation (8)) in the asymptotic limit of infinite frequencies for bodies of any shape. For compact bodies, the boundedness

property also holds in the static limit $\kappa = 0$. For the special case of perfect conductors of compact shape, the boundedness property was proven much earlier for all frequencies [41].

While having a proof of convergence of the MSE is well desirable, from the practical point of view it is of more need to know if the convergence is fast enough for the first few terms of the MSE, in order to provide a good approximation of an entire series. Given the current status of experiments, obtaining the CP energy with an error of less than a percent would be acceptable. To investigate this problem, we consider using as a benchmark the CP interaction of a particle with a body for which the scattering amplitude (T-matrix) is known exactly, and then to verify in such a setup the rate of convergence of the MSE expansion to the energy exact formula. In what follows, choose to study a dielectric sphere and a dielectric cylinder. We consider three different materials: a conductor (gold), a semiconductor (silicon), and an insulator (polystyrene). Since these materials have quite different permittivities, one can check how the rate of convergence of the MSE is affected by the magnitude of the permittivity. We compare the rate of convergence of the MSE for the two cases of choice C1 and C2, of the free coefficients that enter in the definition of the SSO. We Let us denote by $MSE_k, k = 0, 1, \dots$, the estimate of the CP energy corresponding to the inclusion of \mathbb{K} up to the k power into the MSE (3).

4.1. Materials

In the computations here, the following expressions for the permittivities of the materials are used:

$$\epsilon_{\text{Au}}(i\zeta_n) = 1 + \frac{\Omega_p^2}{\zeta(\zeta + \gamma)} + \sum_{j=1}^6 \frac{f_j}{\omega_j^2 + g_j\zeta + \zeta^2}, \tag{10}$$

$$\epsilon_{\text{Si}}(i\zeta_n) = \epsilon_{\infty}^{(\text{Si})} + \frac{\epsilon_0^{(\text{Si})} - \epsilon_{\infty}^{(\text{Si})}}{1 + \zeta^2/\omega_{\text{UV}}^2}, \tag{11}$$

$$\epsilon_{\text{polystyrene}}(i\zeta_n) = 1 + \sum_{j=1}^4 \frac{f_j}{\omega_j^2 + g_j\zeta + \zeta^2}, \tag{12}$$

where $\Omega_p = 9 \text{ eV}/\hbar, \gamma = 0.035 \text{ eV}/\hbar, \epsilon_{\infty}^{(\text{Si})} = 1.035, \epsilon_0^{(\text{Si})} = 11.87$, and $\omega_{\text{UV}} = 4.34 \text{ eV}/\hbar$; the oscillator parameters ω_j, f_j, g_j for Au and polystyrene are listed in Tables 1 and 2, respectively. The particle's polarizability, α , is assumed to be frequency-independent.

Table 1. Oscillator parameteres for Au [54]. See Equation (10).

j	$\omega_j \text{ (eV}/\hbar)$	$f_j \text{ (eV}^2/\hbar^2)$	$g_j \text{ (eV}/\hbar)$
1	3.05	7.091	0.75
2	4.15	41.46	1.85
3	5.4	2.7	1.0
4	8.5	154.7	7.0
5	13.5	44.55	6.0
6	21.5	309.6	9.0

Table 2. Oscillator parameteres for polystyrene [4]. See Equation (12).

j	$\omega_j \text{ (eV}/\hbar)$	$f_j \text{ (eV}^2/\hbar^2)$	$g_j \text{ (eV}/\hbar)$
1	6.35	14.6	0.65
2	14.0	96.9	5.0
3	11.0	44.4	3.5
4	20.1	136.9	11.5

4.2. CP Energy for a Sphere

The scattering approach yields the following Formula [45,46] for the CP interaction energy of a polarizable particle at distance d from the surface of a sphere of radius R in vacuum ($\epsilon_0 = \mu_0 = 1$):

$$E_{\text{CP}}^{(\text{exact})} = \frac{k_B T}{a^2} \sum_{n=0}^{\infty} \kappa_n \alpha(i \zeta_n) \sum_{l=1}^{\infty} (2l+1) \times \left\{ T_l^{\text{HH}}(i \zeta_n) \mathcal{K}_l^2(\kappa_n a) - T_l^{\text{EE}}(i \zeta_n) \left[\mathcal{K}_l'^2(\kappa_n a) + \frac{l(l+1)}{\kappa_n^2 a^2} \mathcal{K}_l^2(\kappa_n a) \right] \right\}, \quad (13)$$

where $a = R + d$, l is the multipole index, $\mathcal{K}_l(x) = x k_l(x)$, $k_l(x) = \sqrt{\frac{2}{\pi x}} K_{l+1/2}(x)$ is the modified spherical Bessel function of the third kind, $\mathcal{K}_l'(x) = d\mathcal{K}_l/dx$, and $T_l^{\text{HH}}, T_l^{\text{EE}}$ are the T-matrix elements (Mie coefficients) of the sphere,

$$T_l^{\text{HH}}(i \zeta) = \frac{\sqrt{\mu/\epsilon} \mathcal{I}_l(\sqrt{\epsilon \mu} \kappa R) \mathcal{I}_l'(\kappa R) - \mathcal{I}_l'(\sqrt{\epsilon \mu} \kappa R) \mathcal{I}_l(\kappa R)}{\mathcal{K}_l(\kappa R) \mathcal{I}_l'(\sqrt{\epsilon \mu} \kappa R) - \sqrt{\mu/\epsilon} \mathcal{I}_l(\sqrt{\epsilon \mu} \kappa R) \mathcal{K}_l'(\kappa R)}, \quad (14)$$

$$T_l^{\text{EE}}(i \zeta) = \frac{\sqrt{\epsilon/\mu} \mathcal{I}_l(\sqrt{\epsilon \mu} \kappa R) \mathcal{I}_l'(\kappa R) - \mathcal{I}_l'(\sqrt{\epsilon \mu} \kappa R) \mathcal{I}_l(\kappa R)}{\mathcal{K}_l(\kappa R) \mathcal{I}_l'(\sqrt{\mu/\epsilon} \kappa R) - \sqrt{\epsilon/\mu} \mathcal{I}_l(\sqrt{\epsilon \mu} \kappa R) \mathcal{K}_l'(\kappa R)}, \quad (15)$$

$$T_l^{\text{EH}}(i \zeta) = T_l^{\text{HE}}(i \zeta) = 0, \quad (16)$$

where $\zeta = \kappa c$, $\mathcal{I}_l(x) = x i_l(x)$, and $\mathcal{I}_l'(x) = d\mathcal{I}_l/dx$, with $i_l(x) = \sqrt{\frac{\pi}{2x}} I_{l+1/2}(x)$ the modified spherical Bessel function of the first kind.

The matrix elements of the SSO \mathbb{K} and the operator \mathbb{M} can be straightforwardly computed in the basis of vector spherical harmonics. The corresponding matrices are both diagonal with respect to multipole indices, (l, m) , $-l \leq m \leq l$, and, in addition, these matrices are independent of m . Therefore, the matrix for \mathbb{K} has the structure of l -dependent 4×4 blocks $K_{p,r,l,m;q,s,l',m'} = \delta_{ll'} \delta_{mm'} K_{p,r;q,s}^{(l)}$, where $r, s = 1, 2$ label the tangential fields $Y_{1,lm}(\hat{r})$ and $Y_{2,lm}(\hat{r})$, introduced in Equation (8.1) of Ref. [42].

In Figures 2–4, we show the ratios of the MSE for the CP energy $E_{\text{CP}}^{(\text{MSE}_k)}$ and the exact result for the CP energy $E_{\text{CP}}^{(\text{exact})}$ obtained from Equation (13) versus d/R for Au, Si, and polystyrene. In the case of Au, a comparison of Figure 2a with Figure 2b shows that the rate of convergence is much faster with the asymmetric choice C2 of the coefficients. Actually, with the C2 choice, MSE_3 already differs from the energy exact values by less than one percent for all displayed separations: specifically, the maximum error is of 0.6% for $d/R = 1$, while for $d/R = 0.03$ the error is as small as 0.1%. In the case of Si, the performance of the choice C1 is better than that for C2. Indeed, with the C1 choice, the maximum error of MSE_4 is 0.8% for $d/R = 0.03$, while the minimum error is 0.2% for $d/R = 1$, while for the choice C2, the maximum error is 3.4% for $d/R = 1$. In the case of polystyrene, the performance of C1 case is amazingly good, since with MSE_3 the maximum error is 0.6% for $d/R = 1$, while for $d/R = 0.04$ the error is as low as 0.003%. For polystyrene, the rate of convergence of (C2) is instead quite poor.

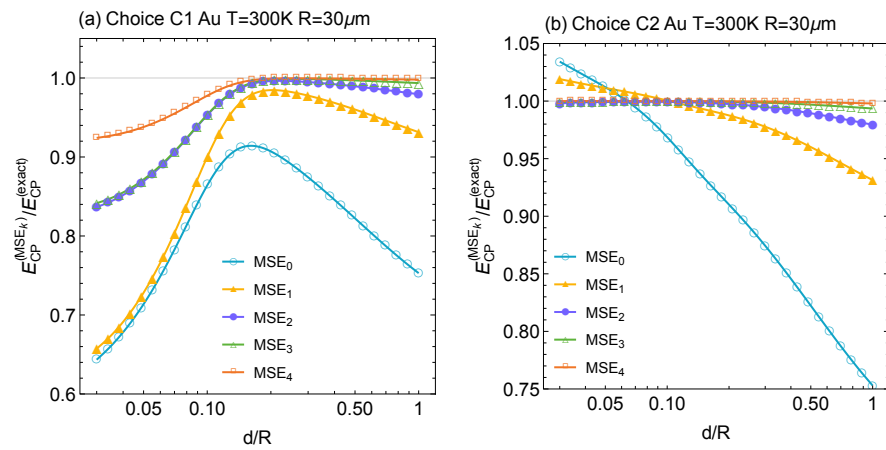


Figure 2. The ratio of MSE of the CP energy (7) up to the k -power of the kernel \mathbb{K} to the energy exact Formula (13) for an Au sphere of radius $R = 30 \mu\text{m}$ at room temperature versus d/R , where d is the distance from the surface, for (a) C1 and (b) C2 choices. See text for details.

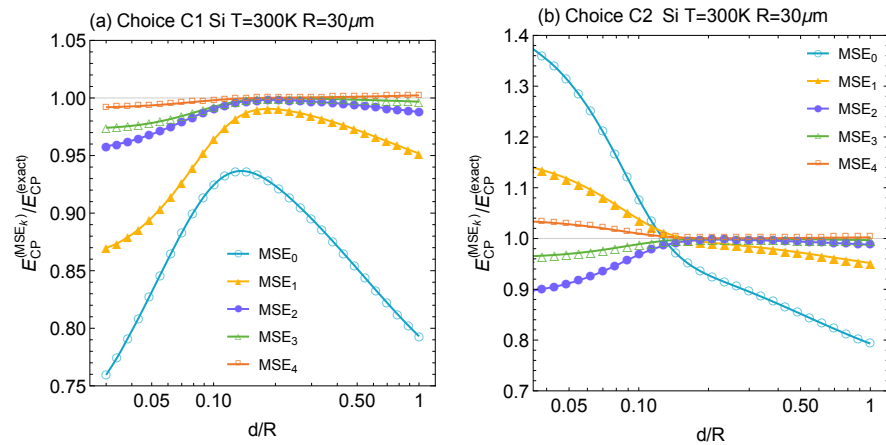


Figure 3. The ratio of MSE of the CP energy (7) up to the k -power of the kernel \mathbb{K} to the energy exact Formula (13) for a Si sphere of radius $R = 30 \mu\text{m}$ at room temperature versus d/R for (a) C1 and (b) C2 choices. See text for details.

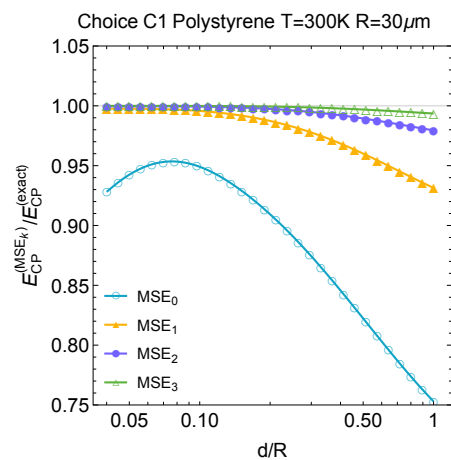


Figure 4. The ratio of MSE of the CP energy (7) up to the k -power of the kernel \mathbb{K} to the energy exact Formula (13) for a polystyrene sphere of radius $R = 30 \mu\text{m}$ at room temperature versus d/R , for C1 choice. See text for details.

4.3. CP Energy for a Cylinder

Within the scattering T-matrix approach, the CP interaction energy of a polarizable particle at distance d from the surface of an infinitely long cylinder of radius R with the permittivity $\epsilon_1 = \epsilon$ permeability $\mu_1 = \mu$ in vacuum ($\epsilon_0 = \mu_0 = 1$) is

$$\begin{aligned}
 E_{\text{CP}}^{(\text{exact})} &= \frac{k_B T}{\pi} \sum_{n=0}^{\infty} \kappa_n^2 \alpha(i\zeta_n) \int_{-\infty}^{\infty} dk_z \sum_{m=-\infty}^{\infty} \quad (17) \\
 &\times \left\{ T_{k_z m}^{\text{EE}}(i\zeta_n) \frac{1}{\kappa_n^2} \left[k_z^2 K_m'^2(p_0 a) + \left(\frac{m^2 k_z^2}{p_0^2 a^2} + p_0^2 \right) K_m^2(p_0 a) \right] \right. \\
 &- T_{k_z m}^{\text{HH}}(i\zeta_n) \left[K_m'^2(p_0 a) + \frac{m^2}{p_0^2 a^2} K_m^2(p_0 a) \right] \\
 &\left. + T_{k_z m}^{\text{EH}}(i\zeta_n) \frac{4mk_z}{\kappa_n p_0 a} K_m(p_0 a) K_m'^2(p_0 a) \right\},
 \end{aligned}$$

where $a = R + d$, $p_0 = \sqrt{\kappa^2 + k_z^2}$, m is the multipole index, K_m is the modified Bessel function of second kind and K_m' its derivative, and $T_{k_z m}^{NM}$, ($N, M \in \{E, H\}$) are the T-matrix elements of a dielectric cylinder [48],

$$T_{k_z m}^{\text{HH}}(i\zeta) = -\frac{I_m(p_0 R)}{K_m(p_0 R)} \frac{\Delta_1 \Delta_4 + Y^2}{\Delta_1 \Delta_2 + Y^2}, \quad (18)$$

$$T_{k_z m}^{\text{EE}}(i\zeta) = -\frac{I_m(p_0 R)}{K_m(p_0 R)} \frac{\Delta_2 \Delta_3 + Y^2}{\Delta_1 \Delta_2 + Y^2}, \quad (19)$$

$$T_{k_z m}^{\text{HE}}(i\zeta) = -T_{k_z m}^{\text{EH}}(i\zeta) = \frac{Y}{\sqrt{\epsilon\mu}(p_0 R)^2 K_m(p_0 R)^2} \frac{1}{\Delta_1 \Delta_2 + Y^2}, \quad (20)$$

with I_m the modified Bessel function of first kind and

$$Y = \frac{mk_z}{\sqrt{\epsilon\mu}R^2\kappa} \left(\frac{1}{p^2} - \frac{1}{p_0^2} \right), \quad (21)$$

with $p = \sqrt{\epsilon\mu\kappa^2 + k_z^2}$ and

$$\Delta_1 = \frac{I_m'(pR)}{pRI_m(pR)} - \frac{1}{\epsilon} \frac{K_m'(p_0 R)}{p_0 RK_m(p_0 R)}, \quad (22)$$

$$\Delta_2 = \frac{I_m'(pR)}{pRI_m(pR)} - \frac{1}{\mu} \frac{K_m'(p_0 R)}{p_0 RK_m(p_0 R)}, \quad (23)$$

$$\Delta_3 = \frac{I_m'(pR)}{pRI_m(pR)} - \frac{1}{\epsilon} \frac{I_m'(p_0 R)}{p_0 RI_m(p_0 R)}, \quad (24)$$

$$\Delta_4 = \frac{I_m'(pR)}{pRI_m(pR)} - \frac{1}{\mu} \frac{I_m'(p_0 R)}{p_0 RI_m(p_0 R)}. \quad (25)$$

To notice is that, in general, the polarization is *not conserved* under scattering, i.e., $T_{k_z m}^{\text{EH}} \neq 0 \neq T_{k_z m}^{\text{HE}}$. This property, together with its quasi-2D shape, makes the cylinder an important benchmark test for the convergence of the MSE.

The CP energy can be straightforwardly obtained as an MSE since the SSO \mathbb{K} and the operator \mathbb{M} can be computed by substituting for the free Green functions in Equations (5) and (6) an expansion in vector cylindrical waves. In Figure 5, we again show the numerical results for the ratio of the MSE for the CP energy $E_{\text{CP}}^{(\text{MSE}_k)}$ at MSE of the order k and the exact result for the CP energy $E_{\text{CP}}^{(\text{exact})}$ obtained from Equation (18). The materials, temperature, and geometric lengths are the same as in the case of a sphere. For Si, one observes that the MSE with the choice case C1 has converged at order MSE₃ to the energy exact calculations

within approximately 3%, with the largest deviations at the shortest (2.4%) and longest (3.3%) considered separation. The deviation is minimal at intermediate distances around $d/R = 0.2$, with an error of only 0.1%. Hence, the performance of the MSE for an infinite cylinder is quite similar to a compact sphere. We do not consider the coefficients from the C2 choice as they performed worse than the choice case C1 for a sphere. For polystyrene, we consider again only the choice case C1, for the same reason. Due to its low dielectric contrast, one expects the choice C1 to give good convergence of the MSE at low orders. Indeed, the rate of convergence is quite fast so that the MSE can be terminated at the order MSE_1 already, with a maximum deviation from the energy exact value of only 1.9% at the separation $d = R$. Let us note that, in general, that with the choice case C1, the lowest order MSE_0 , the estimate of the energy for the cylinder is not as good as that for the sphere. This is presumably due to arbitrarily long-range charge and current fluctuations along the cylinder, which require at least one power of the operator \mathbb{K} to be described properly.

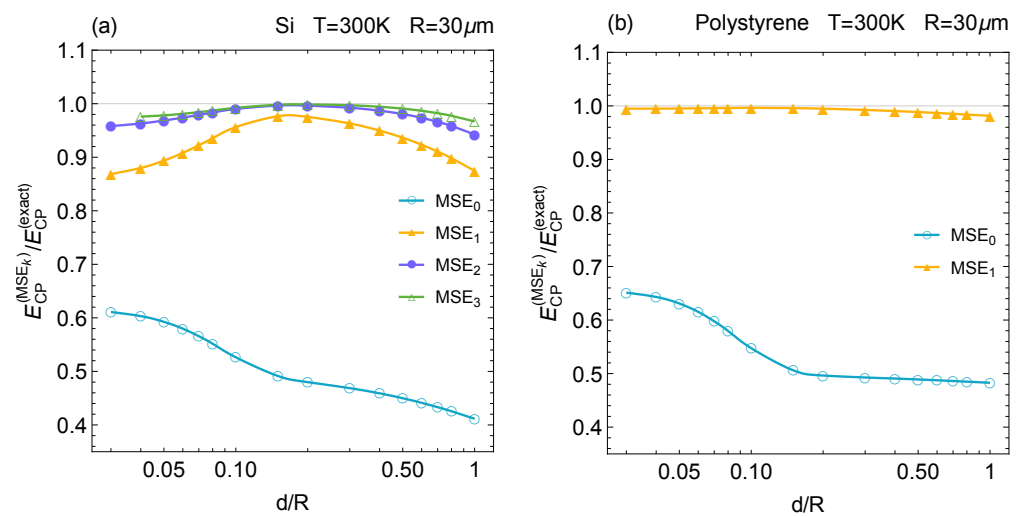


Figure 5. The ratio of MSE of the CP energy (7) up to the k -power of the kernel \mathbb{K} to the energy exact Formula (18) for (a) a Silicon cylinder and (b) a polystyrene cylinder of radius $R = 30 \mu m$ at room temperature $T = 300 K$, for the choice case C1. See text for details.

Finally, it is necessary to discuss the case of a metal, such as Au. As the dielectric function diverges in the limit $\kappa \rightarrow 0$, the classical term $n = 0$ of the Matsubara sum resembles that of a perfect conductor. We have shown that, for a cylinder, the SSO \mathbb{K} , for the choice case C1, in the partial wave channel $m = 0$, has an eigenvalue that approaches unity when $\kappa \rightarrow 0$ and $\epsilon \rightarrow \infty$ [44]. For the choice case C2 the situation is even worse as there is an eigenvalue approaching unity in all partial wave channels. This property is expected to persist for all quasi-2D shapes with a compact cross section. Hence, for such metallic shapes the classical term $n = 0$ cannot be obtained from an MSE. However, the surface scattering approach as developed by us is also useful for zero frequency $\kappa = 0$ as the inverse of $\mathbb{M} = \mathbb{I} - \mathbb{K}$ can be computed directly, without resorting to an MSE. We note that for $\kappa = 0$ the expression for \mathbb{K} simplifies considerably, in particular in the perfect conductor limit [44].

To conclude, we have demonstrated that the MSE provides an especially well-suited tool to compute Casimir–Polder interactions with high precision for a quite wide range of materials. Let us stress that this conclusion is not specific to the shapes considered here but is expected to hold generically for any compact 3D shape or quasi-2D shape. Here, we considered a sphere and a cylinder just because, for those shapes, the exact results are known and hence the convergence of our MSE can be tested. Most essentially, for general shapes where the T-matrix is not known the SSO \mathbb{K} can be computed and the MSE implemented to obtain high precision results for the interaction.

Author Contributions: Both authors contributed equally to this work. All authors have read and agreed to the published version of the manuscript.

Funding: This research received no external funding.

Data Availability Statement: No external data used.

Conflicts of Interest: The authors declare no conflict of interest.

References

1. Casimir, H.B.G. On the attraction between two perfectly conducting plates. *Proc. Kon. Ned. Akad. Wetensch. B* **1948**, *51*, 793–795. Available online: <https://dwc.knaw.nl/DL/publications/PU00018547.pdf> (accessed on 6 January 2024).
2. Lifshitz, E.M. The theory of molecular attractive force between solids. *Sov. Phys. JETP (J. Exp. Theoret. Phys.)* **1956**, *2*, 73–83. Available online: <http://jetp.ras.ru/cgi-bin/e/index/e/2/1/p73?a=list> (accessed on 6 January 2024).
3. Deriaguin, B.V.; Abrikosova, I.I. Direct measurement of the molecular attraction of solid bodies. 1. Statement of the problem and method of measuring forces by using negative feedback. *Sov. Phys. JETP (J. Exp. Theoret. Phys.)* **1957**, *3*, 819–829. Available online: <http://jetp.ras.ru/cgi-bin/e/index/e/3/6/p819?a=list> (accessed on 6 January 2024).
4. Parsegian, V.A. *Van der Waals Forces: A Handbook for Biologists, Chemists, Engineers, and Physicists*; Cambridge University Press: New York, NY, USA, 2006. [CrossRef]
5. Klimchitskaya, G.L.; Mohideen, U.; Mostepanenko, V.M. The Casimir force between real materials: Experiment and theory. *Rev. Mod. Phys.* **2009**, *81*, 1827–1885. [CrossRef]
6. Buhmann, S.Y. *Dispersion Forces. I: Macroscopic Quantum Electrodynamics and Ground-State Casimir, Casimir–Polder, and van der Waals Forces*; Springer: Berlin/Heidelberg, Germany, 2012. [CrossRef]
7. Rodriguez, A.W.; Hui, P.C.; Wolf, D.P.; Johnson, S.G.; Loncar, M.; Capasso, F. Classical and fluctuation-induced electromagnetic interactions in micron-scale systems: Designer bonding, antibonding, and Casimir forces. *Ann. Phys.* **2014**, *527*, 45. [CrossRef]
8. Woods, L.M.; Dalvit, D.A.R.; Tkatchenko, A.; Rodriguez-Lopez, P.; Rodriguez, A.W.; Podgornik, R. Materials perspective on Casimir and van der Waals interactions. *Rev. Mod. Phys.* **2016**, *88*, 045003. [CrossRef]
9. Bimonte, G.; Emig, T.; Kardar, M.; Krüger, M. Nonequilibrium fluctuational quantum electrodynamics: Heat radiation, heat transfer, and force. *Annu. Rev. Condens. Matter Phys.* **2017**, *8*, 119–143. [CrossRef]
10. Langbein, D. *Theory of van der Waals Attraction*; Springer: Berlin, Heidelberg, Germany, 1974. [CrossRef]
11. Lamoreaux, S.K. Demonstration of the Casimir force in the 0.6 to 6 μm range. *Phys. Rev. Lett.* **1997**, *78*, 5–8. [CrossRef]
12. Mohideen, U.; Roy, A. Precision measurement of the Casimir force from 0.1 to 0.9 μm . *Phys. Rev. Lett.* **1998**, *81*, 4549–4552. [CrossRef]
13. Chan, H.B.; Aksyuk, V.A.; Kleiman, R.N.; Bishop, D.J.; Capasso, F. Quantum mechanical actuation of microelectromechanical systems by the Casimir force. *Science* **2001**, *291*, 1941–1944. [CrossRef]
14. Bressi, G.; Carugno, G.; Onofrio, R.; Ruoso, G. Measurement of the Casimir force between parallel metallic surfaces. *Phys. Rev. Lett.* **2002**, *88*, 041804. [CrossRef]
15. Decca, R.S.; López, D.; Fischbach, E.; Krause, D.E. Measurement of the Casimir force between dissimilar metals. *Phys. Rev. Lett.* **2003**, *91*, 050402. [CrossRef]
16. Munday, J.N.; Capasso, F.; Parsegian, V.A. Measured long-range repulsive Casimir–Lifshitz forces. *Nature* **2009**, *457*, 170–173. [CrossRef] [PubMed]
17. Sushkov, A.O.; Kim, W.J.; Dalvit, D.A.R.; Lamoreaux, S.K. Observation of the thermal Casimir force. *Nat. Phys.* **2011**, *7*, 230–233. [CrossRef]
18. Tang, L.; Wang, M.; Ng, C.Y.; Nikolic, M.; Chan, C.T.; Rodriguez, A.W.; Chan, H.B. Measurement of non-monotonic Casimir forces between silicon nanostructures. *Nat. Photon.* **2017**, *11*, 97–101. [CrossRef]
19. Emig, T.; Graham, N.; Jaffe, R.L.; Kardar, M. Casimir forces between arbitrary compact objects. *Phys. Rev. Lett.* **2007**, *99*, 170403. [CrossRef] [PubMed]
20. Kenneth, O.; Klich, I. Casimir forces in a T-operator approach. *Phys. Rev. B* **2008**, *78*, 014103. [CrossRef]
21. Rahi, S.J.; Emig, T.; Graham, N.; Jaffe, R.L.; Kardar, M. Scattering theory approach to electrodynamic Casimir forces. *Phys. Rev. D* **2009**, *80*, 085021. [CrossRef]
22. Genet, C.; Lambrecht, A.; Reynaud, S. Casimir force and the quantum theory of lossy optical cavities. *Phys. Rev. A* **2003**, *67*, 043811. [CrossRef]
23. Lambrecht, A.; Maia Neto, P.A.; Reynaud, S. The Casimir effect within scattering theory. *New J. Phys.* **2006**, *8*, 243. [CrossRef]
24. Maghrebi, M.F.; Rahi, S.J.; Emig, T.; Graham, N.; Jaffe, R.L.; Kardar, M. Analytical results on Casimir forces for conductors with edges and tips. *Proc. Natl. Acad. Sci. USA* **2011**, *108*, 6867–6871. [CrossRef]
25. Bimonte, G.; Emig, T. Exact results for classical Casimir interactions: Dirichlet and Drude model in the sphere-sphere and sphere-plane geometry. *Phys. Rev. Lett.* **2012**, *109*, 160403. [CrossRef] [PubMed]
26. Schoger, T.; Ingold, G.L. Classical Casimir free energy for two Drude spheres of arbitrary radii: A plane-wave approach. *SciPost Phys. Core* **2021**, *4*, 011. [CrossRef]

27. Hartmann, M.; Ingol, G.L.; Maia Neto, P.A. Plasma versus Drude modeling of the Casimir force: Beyond the proximity force approximation. *Phys. Rev. Lett.* **2017**, *119*, 043901. [[CrossRef](#)] [[PubMed](#)]
28. Wang, M.; Tang, L.; Ng, C.Y.; Messina, R.; Guizal, B.; Crosse, J.A.; Antezza, M.; Chan, C.T.; Chan, H.B. Strong geometry dependence of the Casimir force between interpenetrated rectangular gratings. *Nat. Commun.* **2021**, *12*, 600. [[CrossRef](#)]
29. Banishev, A.A.; Wagner, J.; Emig, T.; Zandi, R.; Mohideen, U. Demonstration of angle-dependent Casimir force between corrugations. *Phys. Rev. Lett.* **2013**, *110*, 250403. [[CrossRef](#)]
30. Intravaia, F.; Koev, S.; Jung, I.W.; Talin, A.A.; Davids, P.S.; Decca, R.S.; Aksyuk, V.A.; Dalvit, D.A.R.; López, D. Strong Casimir force reduction through metallic surface nanostructuring. *Nat. Commun.* **2013**, *4*, 2515. [[CrossRef](#)]
31. Lambrecht, A.; Marachevsky, V.N. Casimir interaction of dielectric gratings. *Phys. Rev. Lett.* **2008**, *101*, 160403. [[CrossRef](#)]
32. Bender, H.; Stehle, C.; Zimmermann, C.; Slama, S.; Fiedler, J.; Scheel, S.; Buhmann, S.Y.; Marachevsky, V.N. Probing atom-surface interactions by diffraction of Bose-Einstein condensates. *Phys. Rev. X* **2014**, *4*, 011029. [[CrossRef](#)]
33. Antezza, M.; Chan, H.; Guizal, B.; Marachevsky, V.N.; Messina, R.; Wang, M. Giant Casimir torque between rotated gratings and the $\theta = 0$ anomaly. *Phys. Rev. Lett.* **2020**, *124*, 013903. [[CrossRef](#)]
34. Fosco, C.D.; Lombardo, F.C.; Mazzitelli, F.D. Proximity force approximation for the Casimir energy as a derivative expansion. *Phys. Rev. D* **2011**, *84*, 105031. [[CrossRef](#)]
35. Bimonte, G.; Emig, T.; Jaffe, R.L.; Kardar, M. Casimir forces beyond the proximity approximation. *Europhys. Lett. (EPL)* **2012**, *97*, 50001. [[CrossRef](#)]
36. Bimonte, G.; Emig, T.; Kardar, M. Material dependence of Casimir forces: Gradient expansion beyond proximity. *Appl. Phys. Lett.* **2012**, *100*, 074110. [[CrossRef](#)]
37. Bimonte, G. Going beyond PFA: A precise formula for the sphere-plate Casimir force. *Europhys. Lett.* **2017**, *118*, 20002. [[CrossRef](#)]
38. Reid, M.T.H.; White, J.; Johnson, S.G. Fluctuating surface currents: An algorithm for efficient prediction of Casimir interactions among arbitrary materials in arbitrary geometries. *Phys. Rev. A* **2013**, *88*, 022514. [[CrossRef](#)]
39. Chew, W.C.; Tong, M.S.; Hu, B. *Integral Equations Methods for Electromagnetic and Elastic Waves*; Springer Nature Switzerland AG: Cham, Switzerland, 2022. [[CrossRef](#)]
40. Volakis, S.K.; Sertel, K. *Integral Equations Methods for Electromagnetics*; SciTech Publishing: Raleigh, NC, USA, 2012.
41. Balian, R.; Duplantier, B. Electromagnetic waves near perfect conductors. I. Multiple scattering expansions. Distribution of modes. *Ann. Phys.* **1977**, *104*, 300–335. [[CrossRef](#)]
42. Balian, R.; Duplantier, B. Electromagnetic waves near perfect conductors. II. Casimir effect. *Ann. Phys.* **1978**, *112*, 165–208. [[CrossRef](#)]
43. Emig, T.; Bimonte, G. Multiple scattering expansion for dielectric Media: Casimir effect. *Phys. Rev. Lett.* **2023**, *130*, 200401. [[CrossRef](#)]
44. Bimonte, G.; Emig, T. Casimir and Casimir-Polder interactions for magneto-dielectric materials: Surface scattering expansion. *Phys. Rev. A* **2023**, *108*, 052807. [[CrossRef](#)]
45. Marachevsky, V.N. Casimir effect and quantum field theory in dielectrics. *Theor. Math. Phys.* **2002**, *131*, 468–482. [[CrossRef](#)]
46. Buhmann, S.Y.; Dung, H.T.; Welsch, D.G. The van der Waals energy of atomic systems near absorbing and dispersing bodies. *J. Opt. B Quantum Semiclass. Opt.* **2004**, *6*, S127–S135. [[CrossRef](#)]
47. Milton, K.A.; Parashar, P.; Pourtolami, N. Casimir-Polder repulsion: Polarizable atoms, cylinders, spheres and ellipsoids. *Phys. Rev. D* **2012**, *85*, 025008. [[CrossRef](#)]
48. Noruzifar, E.; Emig, T.; Mohideen, U.; Zandi, R. Collective charge fluctuations and Casimir interactions for quasi-one-dimensional metals. *Phys. Rev. B* **2012**, *86*, 115449. [[CrossRef](#)]
49. Contreras-Reyes, A.M.; Guérout, R.; Neto, P.A.M.; Dalvit, D.A.R.; Lambrecht, A.; Reynaud, S. Casimir-Polder interaction between an atom and a dielectric grating. *Phys. Rev. A* **2010**, *82*, 052517. [[CrossRef](#)]
50. Bimonte, G.; Emig, T.; Kardar, M. Casimir-Polder interaction for gently curved surfaces. *Phys. Rev. D* **2014**, *90*, 081702. [[CrossRef](#)]
51. Bimonte, G.; Emig, T.; Kardar, M. Casimir-Polder force between anisotropic nanoparticles and gently curved surfaces. *Phys. Rev. D* **2015**, *92*, 025028. [[CrossRef](#)]
52. Kristensen, P.T.; Beverungen, B.; Intravaia, F.; Busch, K. High-accuracy Casimir-Polder force calculations using the discontinuous Galerkin time-domain method. *Phys. Rev. B* **2023**, *108*, 205424. [[CrossRef](#)]
53. Müller, C. *Foundations of the Mathematical Theory of Electromagnetic Waves*; Springer: Berlin/Heidelberg, Germany, 1969. [[CrossRef](#)]
54. Decca, R.S.; Lopez, D.; Fischbach, E.; Klimchitskaya, G.K.; Krause, D.E.; Mostepanenko, V.M. Novel constraints on light elementary particles and extra-dimensional physics from the Casimir effect. *Eur. Phys. J. C* **2007**, *51*, 963–975. [[CrossRef](#)]

Disclaimer/Publisher’s Note: The statements, opinions and data contained in all publications are solely those of the individual author(s) and contributor(s) and not of MDPI and/or the editor(s). MDPI and/or the editor(s) disclaim responsibility for any injury to people or property resulting from any ideas, methods, instructions or products referred to in the content.